Supplement of Atmos. Chem. Phys., 16, 8831–8847, 2016
http://www.atmos-chem-phys.net/16/8831/2016/
doi:10.5194/acp-16-8831-2016-supplement

Atmospheric Chemistry and Physics Open Access EGU

Supplement of

Aerosol source apportionment from 1-year measurements at the CESAR tower in Cabauw, the Netherlands

Patrick Schlag et al.

Correspondence to: Patrick Schlag (p.schlag@fz-juelich.de)

Determination of the Collection Efficiency (CE) algorithm according to Mensah et al. (2012):

1. $CE = 0.5$ for $MF_{NO3} < 0.3$
2. $CE = 1.0$ for $MF_{NO3} \geq 0.78$
3. $CE = 0.1875 + 1.0417 \times MF_{NO3}$ for $0.3 < MF_{NO3} < 0.78$,

with MF_{NO3} = Mass fraction of ammonium nitrate to total PM_1 mass as measured by the ACSM.

Table S1: Overview of the ambient temperatures and relative humidities during the ACSM campaign, measured at 2 m height.

	Period	Minimum	Maximum	Average
Temperature [°C]	1 (11.07.-30.09.2012)	6.7	32.2	16.5
	2 (01.10.-29.12.2012)	-6.1	21.3	7.7
	3 (08.01.-15.02.2013)	-12.3	12.4	0.6
	4 (18.02.-25.04.2013)	-5.1	19.5	3.5
	5 (25.04.-03.06.2013)	2.9	22.3	10.9
	Entire campaign			9.2
Relative Humidity [%]	1 (11.07.-30.09.2012)	35.7	100.6	79.3
	2 (01.10.-29.12.2012)	51.3	102.6	88.6
	3 (08.01.-15.02.2013)	58.9	102.9	86.2
	4 (18.02.-25.04.2013)	23.2	101.2	72.5
	5 (25.04.-03.06.2013)	35.9	100.3	80.2
	Entire campaign			82.2

Table S2: Number of data points, fractional abundances of individual aerosol species in % and the average total mass concentrations (Avg) in µg m^{-3}, for each month and for the entire campaign.

Month	Data points	eBC	Org	NO_3	SO_4	NH_4	Chl	Avg
July 2012	865	5	35	30	15	14	1	6.2
August 2012	1626	6	35	37	9	12	1	4.9
September 2012	1147	8	33	32	11	13	3	8.3
October 2012	1621	9	34	34	9	12	2	7.0
November 2012	1297	8	34	33	9	12	4	7.5
December 2012	1144	6	29	40	8	13	4	7.8
January 2013	962	3	27	44	11	14	1	21.5
February 2013	1269	2	27	42	12	16	1	11.6
March 2013	736	-	29	44	9	16	2	11.9
April 2013	749	-	23	49	10	16	2	11.6
May-June 2013	1841	5	26	39	12	16	2	10.3
Entire campaign	13266	5	35	30	15	14	1	6.2

Table S3: Fractional abundances of ACSM PMF factors observed for each season and for the entire campaign in % and the respective average organic mass concentrations (Org-Avg) in µg m^{-3}. For the constrained profiles HOA and BBOA, the applied a-value is written in brackets.

Period	HOA	BBOA	OOA	HULIS	Org-Avg
Summer 2012 (11.07.-30.09.2012)	16 (a=0.1)	-	37	47	2.1
Autumn 2012 (01.10.-29.12.2012)	14 (a=0.1)	23 (a=0.2)	21	43	2.4
Winter 2013 (08.01.-27.03.2013)	10 (a=0.1)	15 (a=0.3)	48	27	4.1
Spring 2013 (05.04.-03.06.2013)	8 (a=0.1)	9 (a=0.3)	47	36	2.7
Entire campaign	12	13	38	37	2.8

Table S4: Correlation coefficients (Pearson-R^2) of the comparison between ACSM PMF factor and tracer time series over the entire campaign. Highest important correlation coefficients are written in bold values.

Tracer	HOA	BBOA	OOA	HULIS
NO_3	0.28	0.24	**0.63**	0.39
SO_4	0.14	0.23	**0.48**	0.41
$NO_3 + SO_4$	0.27	0.26	**0.67**	0.41
NH_4	0.25	0.23	**0.63**	0.44
Chl	0.14	0.13	0.04	0.10
eBC	0.38	0.39	0.34	**0.47**
m/z 60 (ACSM)	0.42	**0.94**	0.39	0.26
Rn (gas phase, 20 m height)	0.30	0.21	0.23	**0.34**
CO_2 (gas phase, 20 m height)	0.24	**0.31**	0.24	0.21
NO_x (gas phase)	**0.47**	0.36	0.07	0.10
CO (gas phase)	**0.47**	**0.49**	0.37	0.30

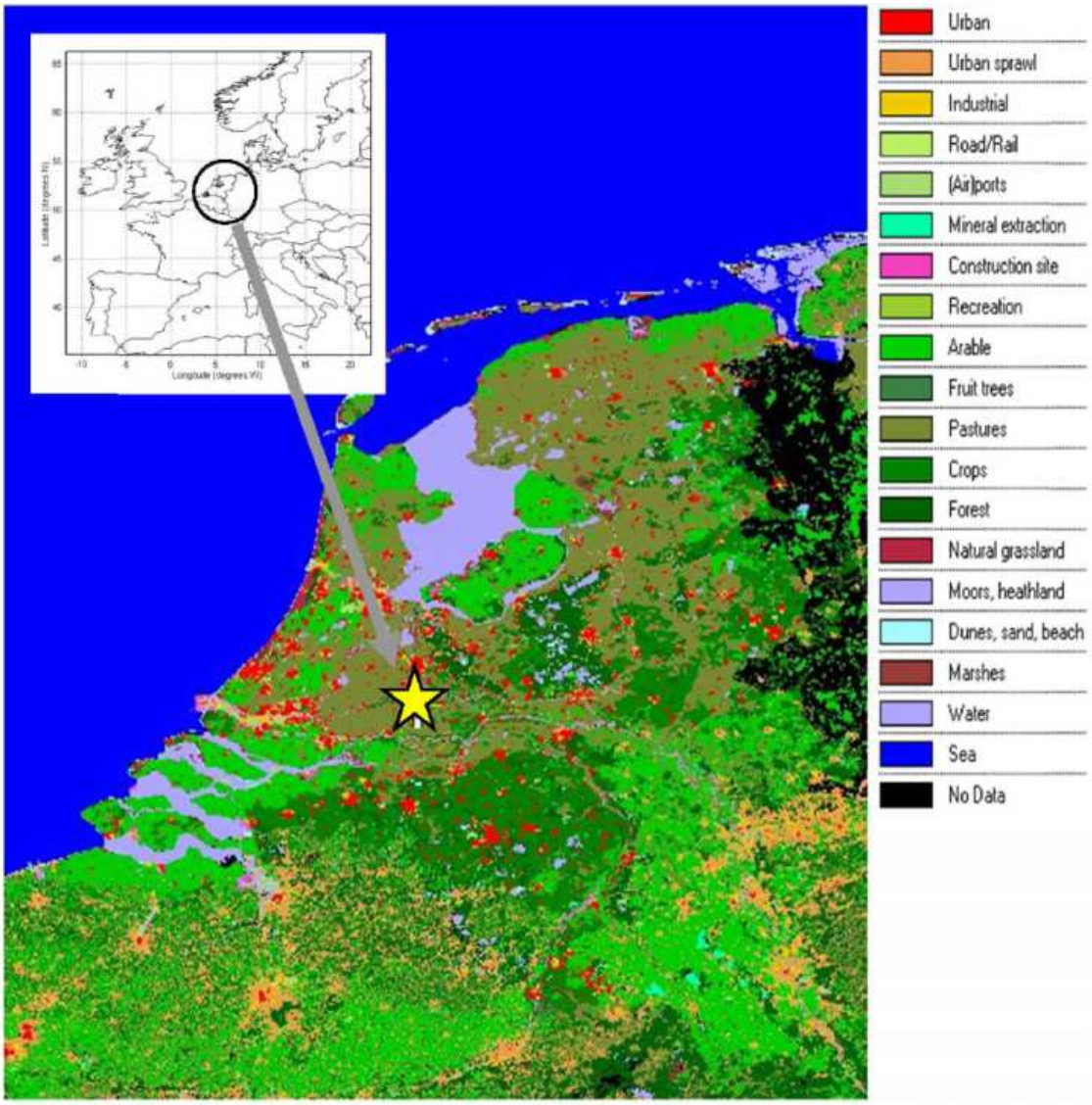

Figure S1: Measurement location; colours define different land use; taken from Vermeulen et al. (2011)

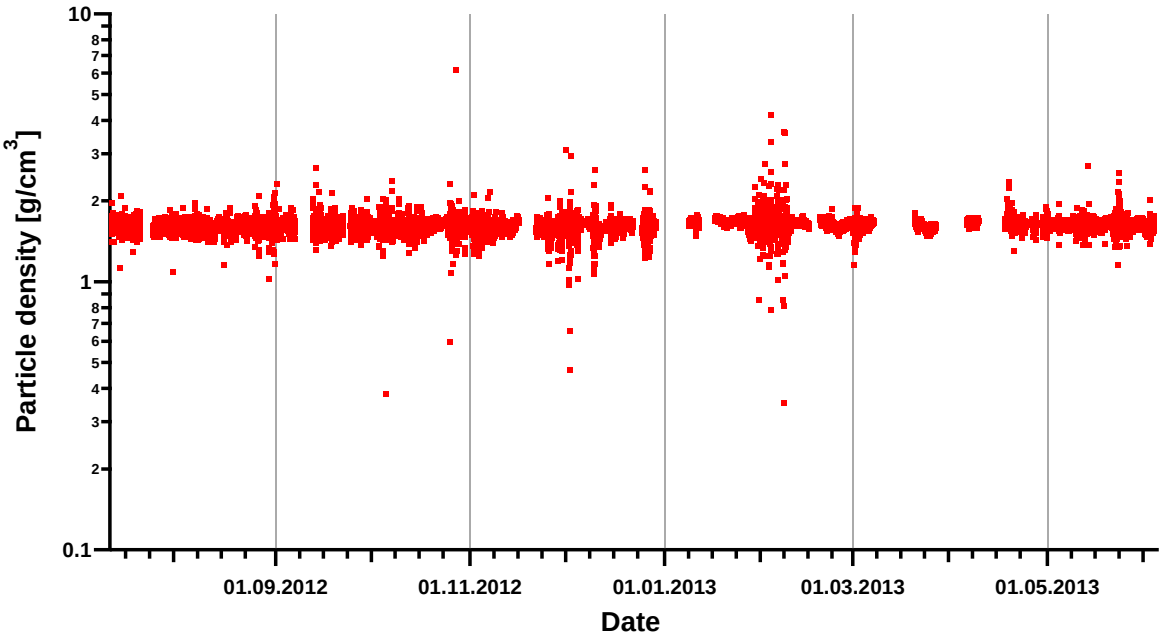

Figure S2: Particle density, determined from ACSM+MAAP aerosol composition as described in Sec. 3.2 in the main text.

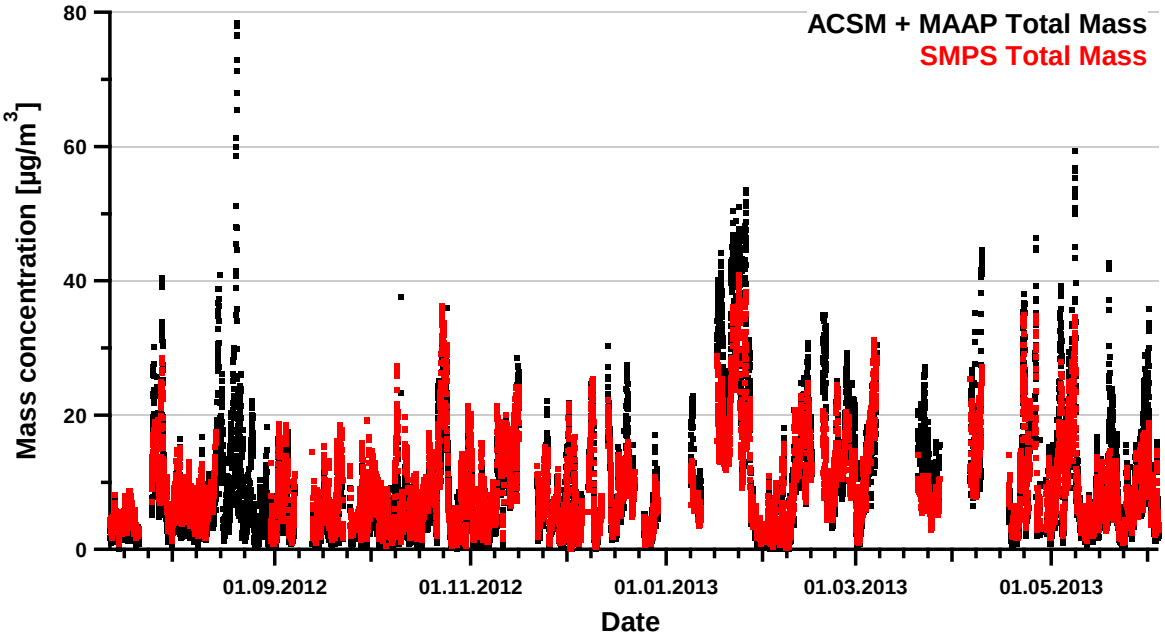

Figure S3: Time series of ACSM+MAAP and SMPS mass concentrations

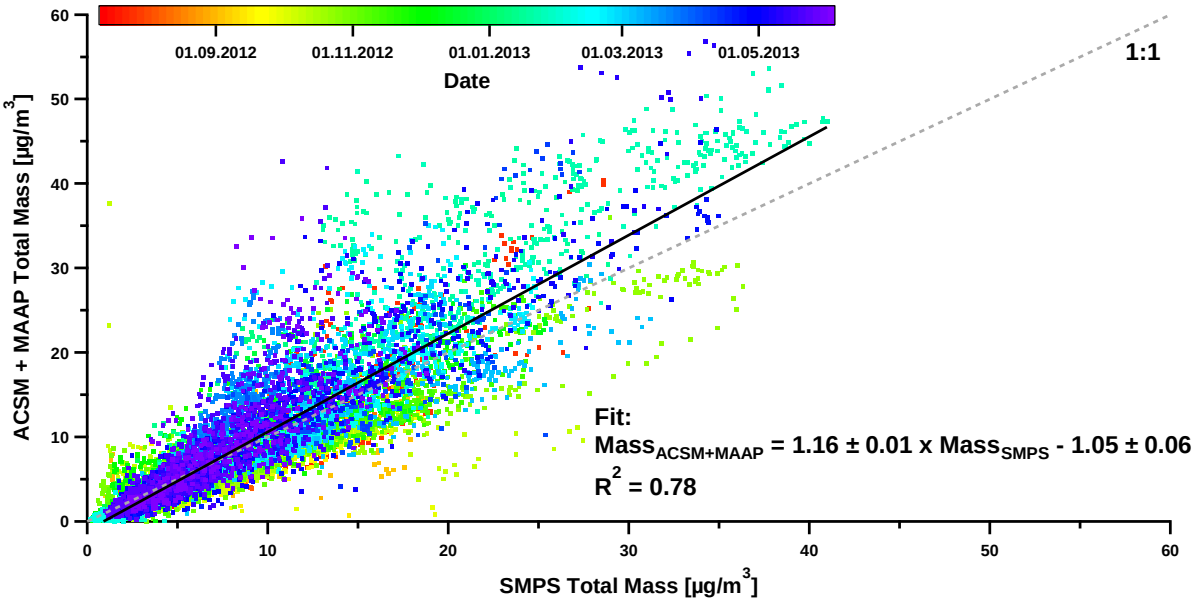

Figure S4: Correlation plot of ACSM+MAAP and SMPS mass concentrations

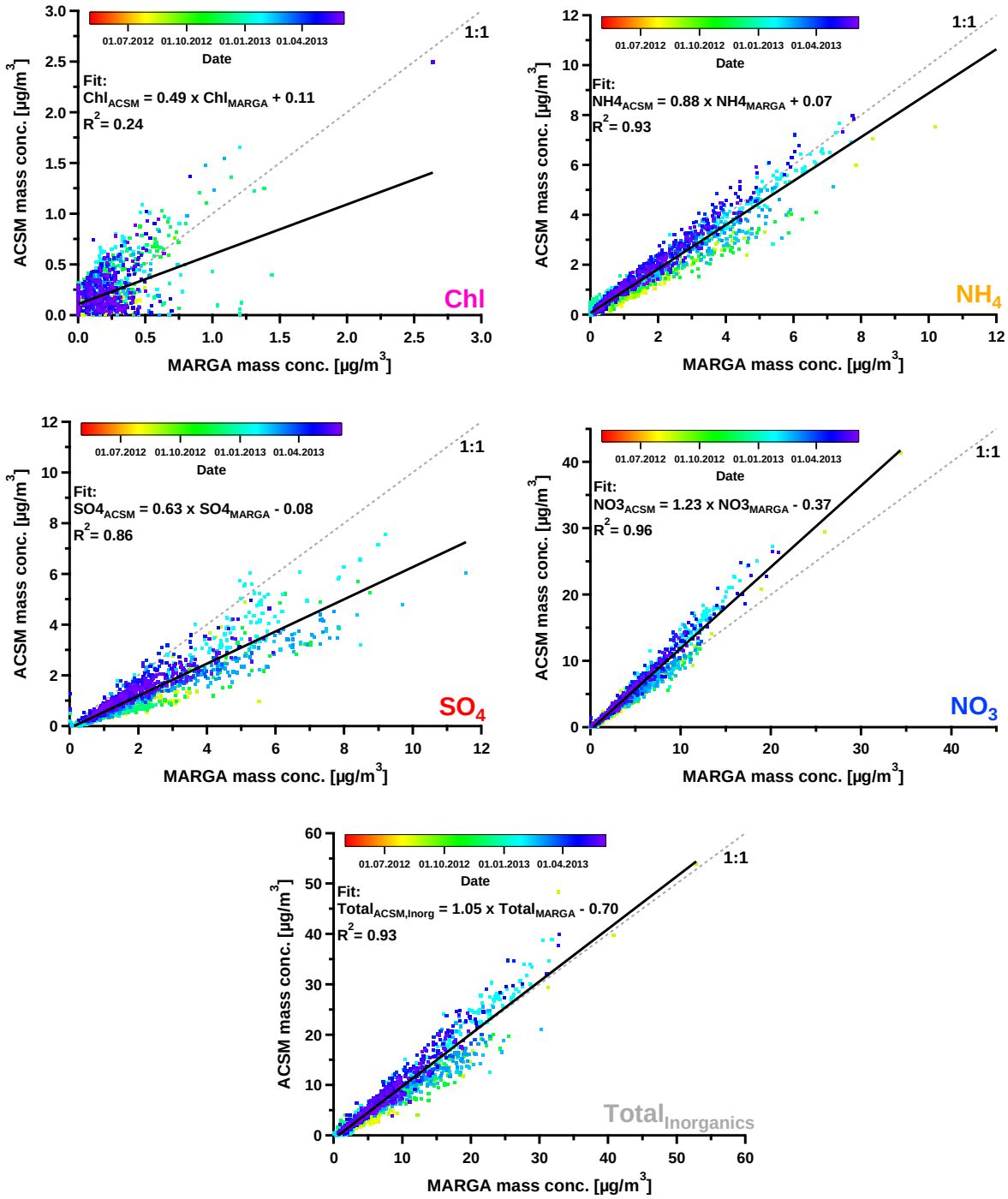

Figure S5: Correlation graphs of Chl, NH_4, SO_4, NO_3, and total inorganic mass concentrations from ACSM and MARGA PM_1 data

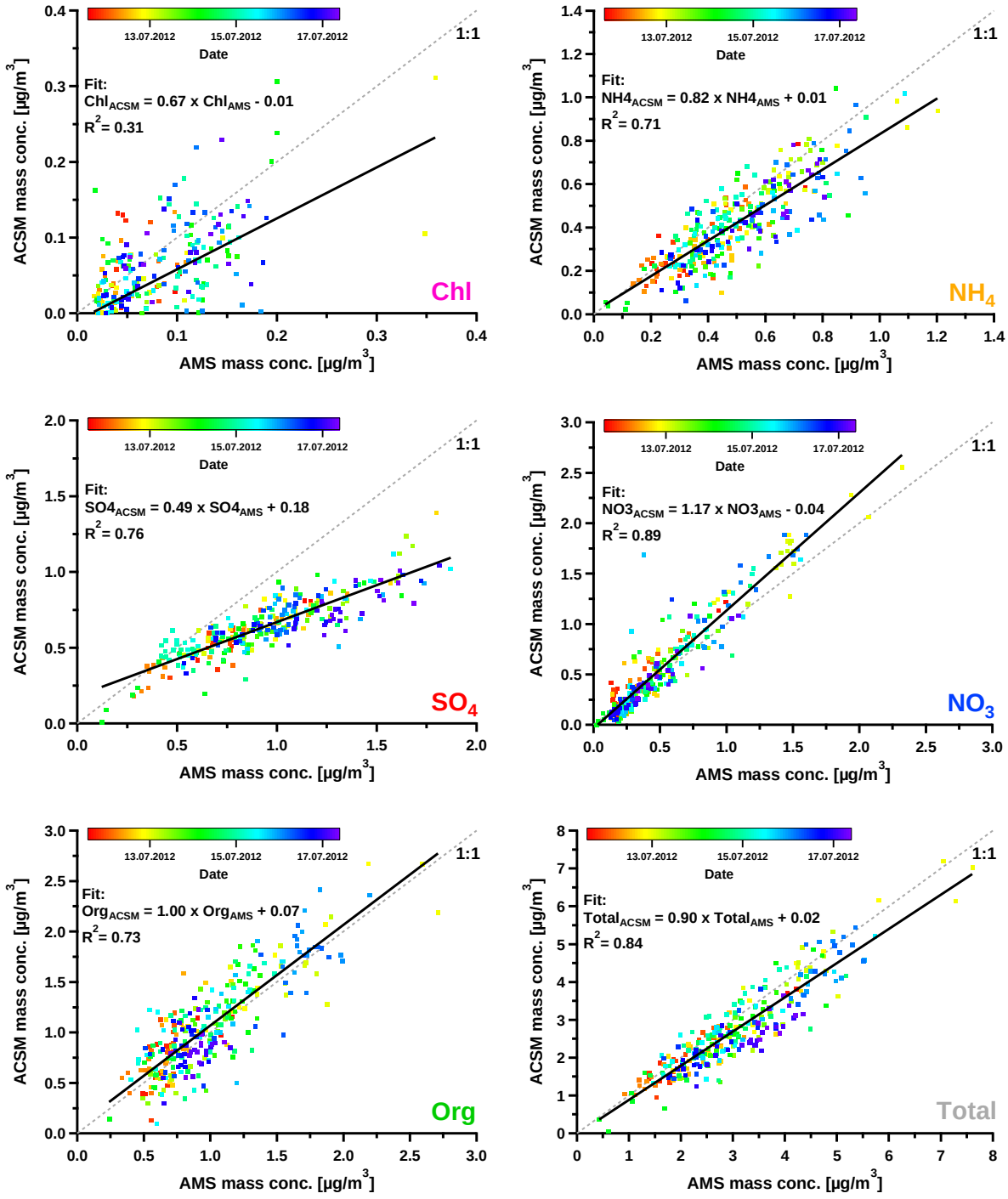

Figure S6: Correlation graphs of individual species and total mass concentrations from ACSM data with AMS data

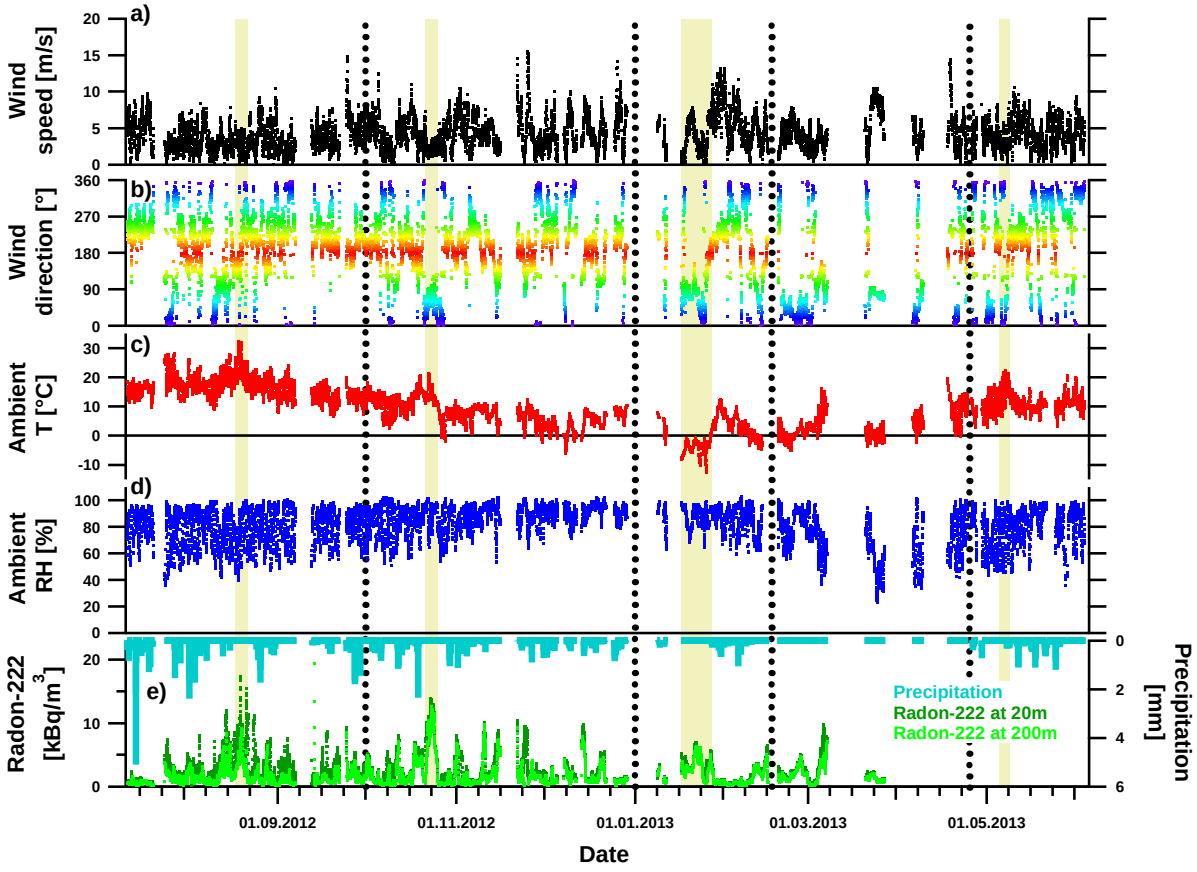

Figure S7: Meteorological overview of the ACSM campaign: a) Wind speed at 10 m height. b) Wind direction (0°/360°, 90°, 180°, and 270° represent North, East, South, and West, respectively; for a better clearance the graph is additionally color-coded by degrees). c) and d) temperature and relative humidity at 2 m height. e) Precipitation and Radon-222, measured at 20 m and 200 m. Pollution events are indicated by shaded areas.

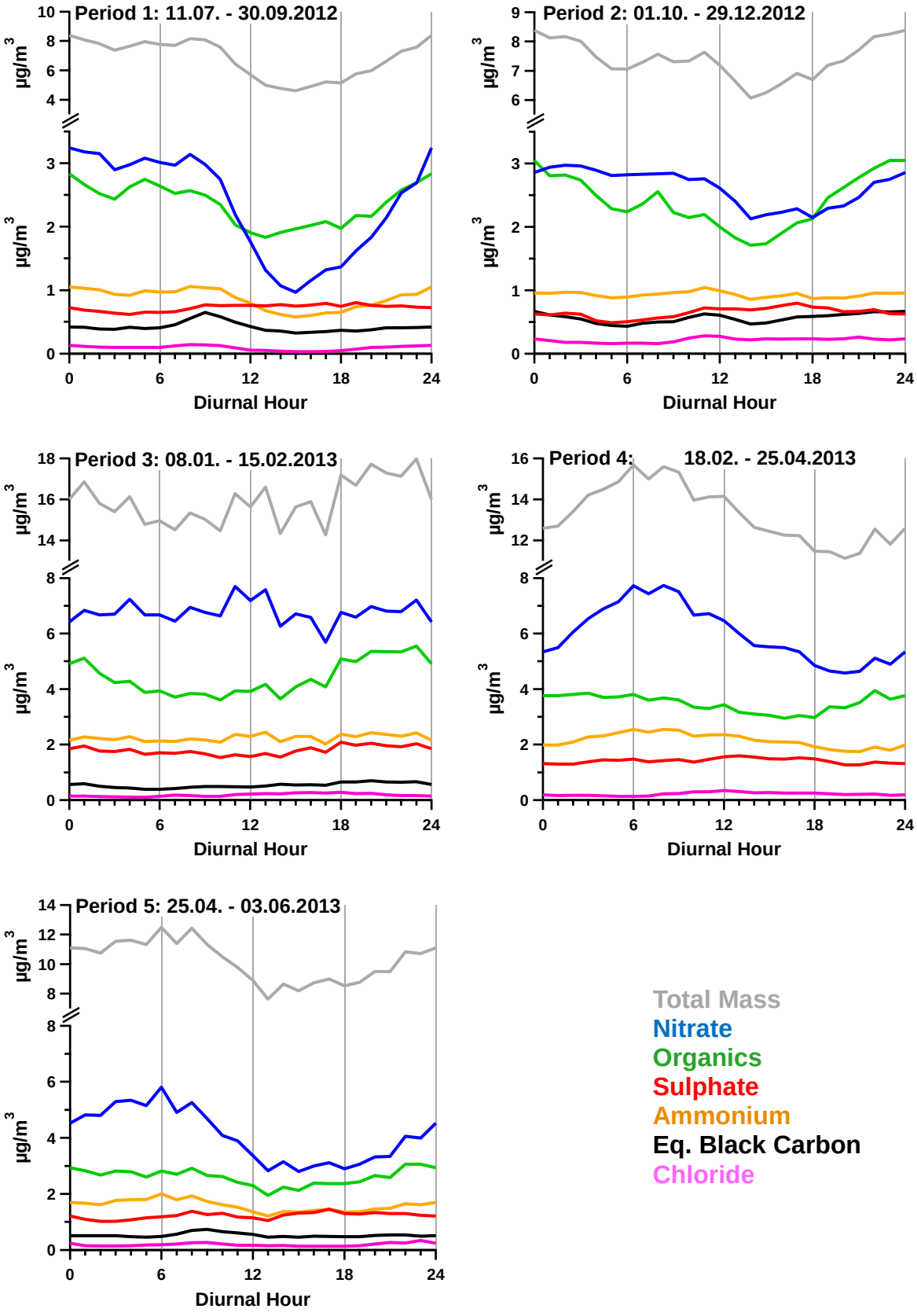

Figure S8: Diurnal variation (local time) of individual species and the total mass, averaged over the entire ACSM campaign and over the five periods, which are explained in Table S1. Note the different scales of y-axes between the periods.

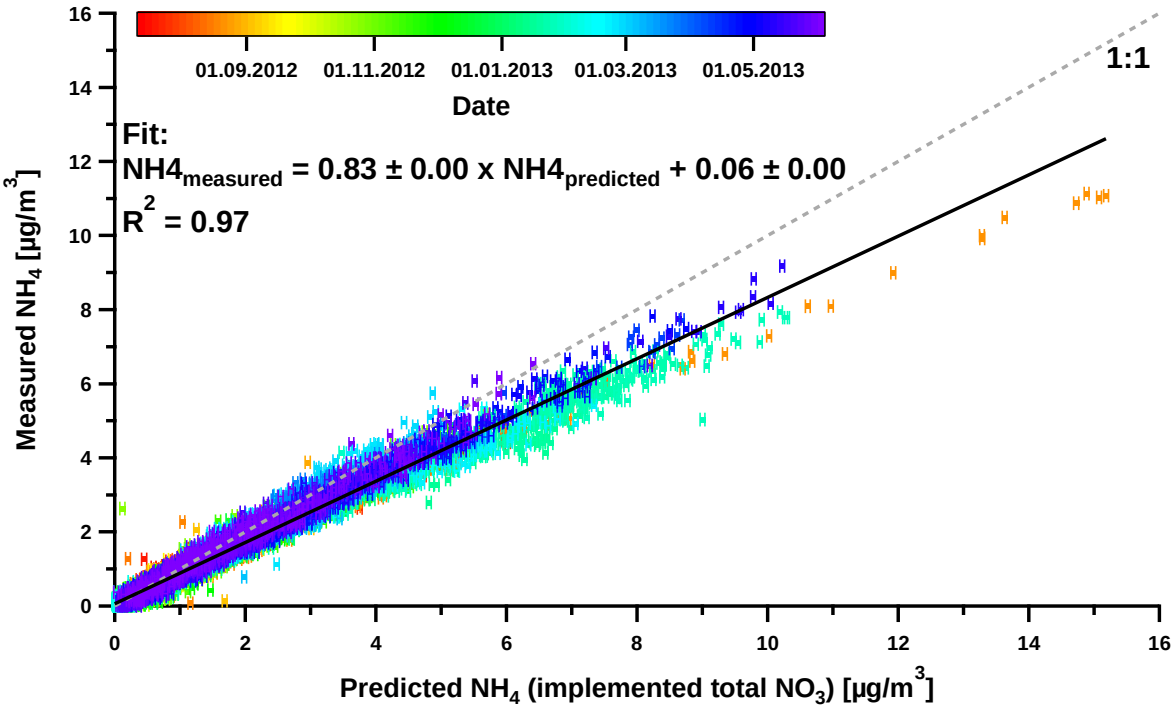

Figure S9: Correlation plot of measured against predicted NH_4 during the ACSM campaign. Error bars represent uncertainties of the NH_4 prediction.

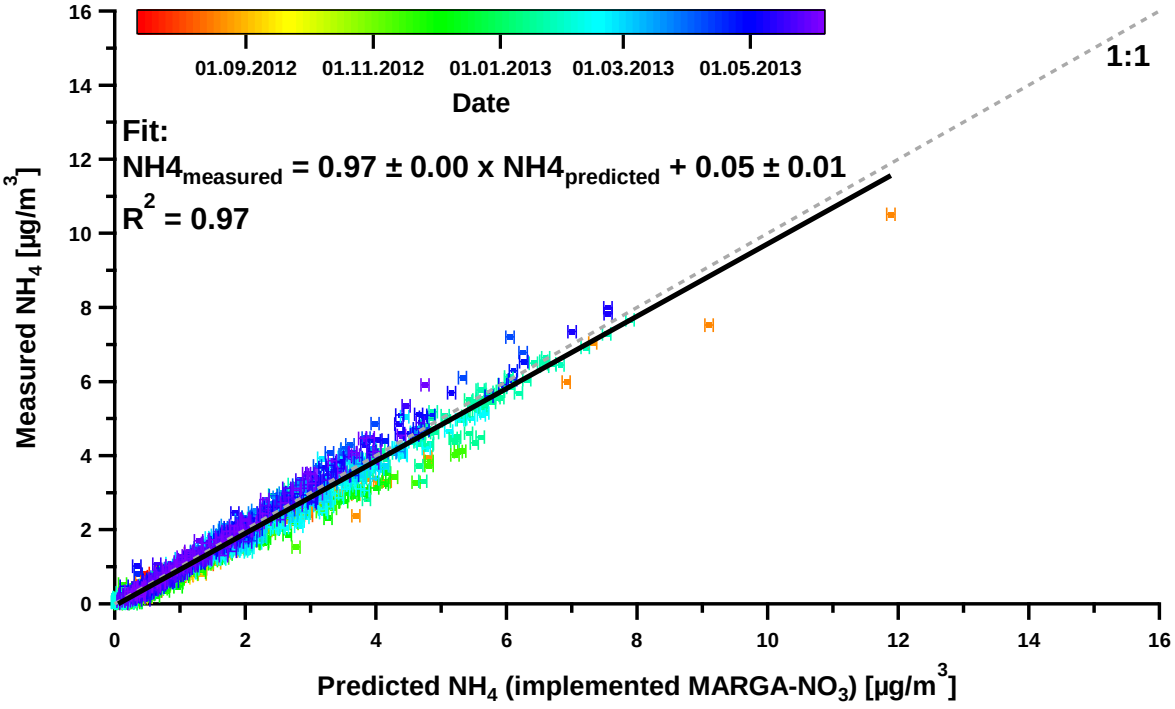

Figure S10: Correlation plot of measured against predicted NH_4 during the ACSM campaign. Here, the MARGA-NO_3 instead of the ACSM-NO_3 was used for the ion balance. Therefore, all time series were averaged to MARGA time prior to the correlation. Error bars represent uncertainties of the NH_4 prediction.

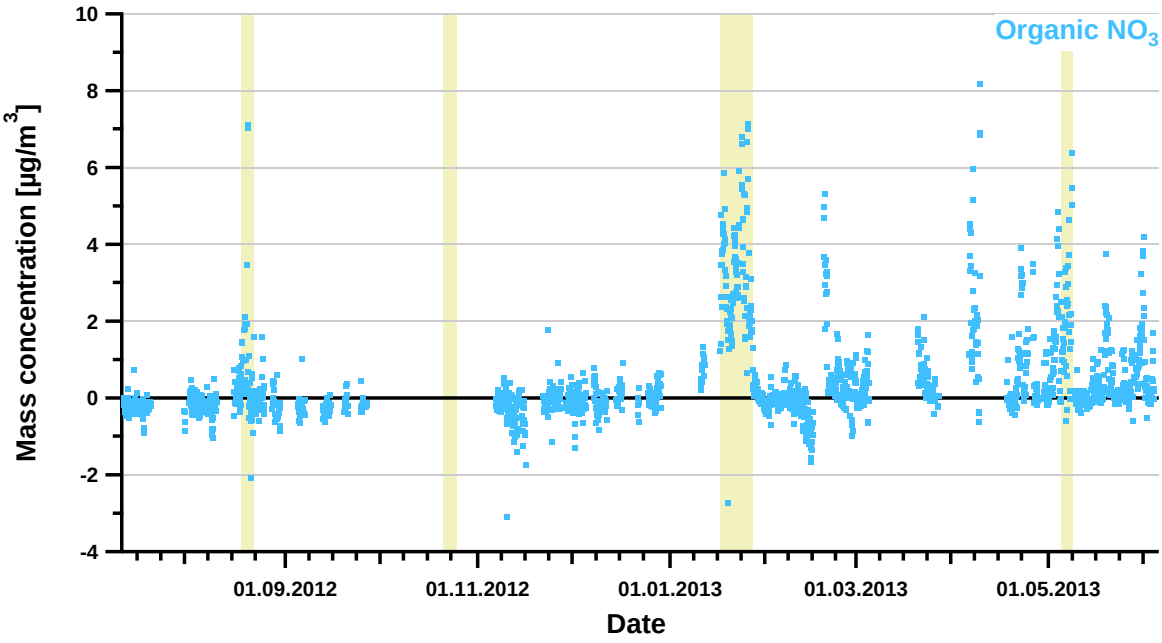

Figure S11: Time series of the ACSM organic nitrate mass concentrations, calculated by subtracting the MARGA-NO_3 from the ACSM-NO_3, according to Sec. 3.2 in the main text. Pollution events are indicated by shaded areas.

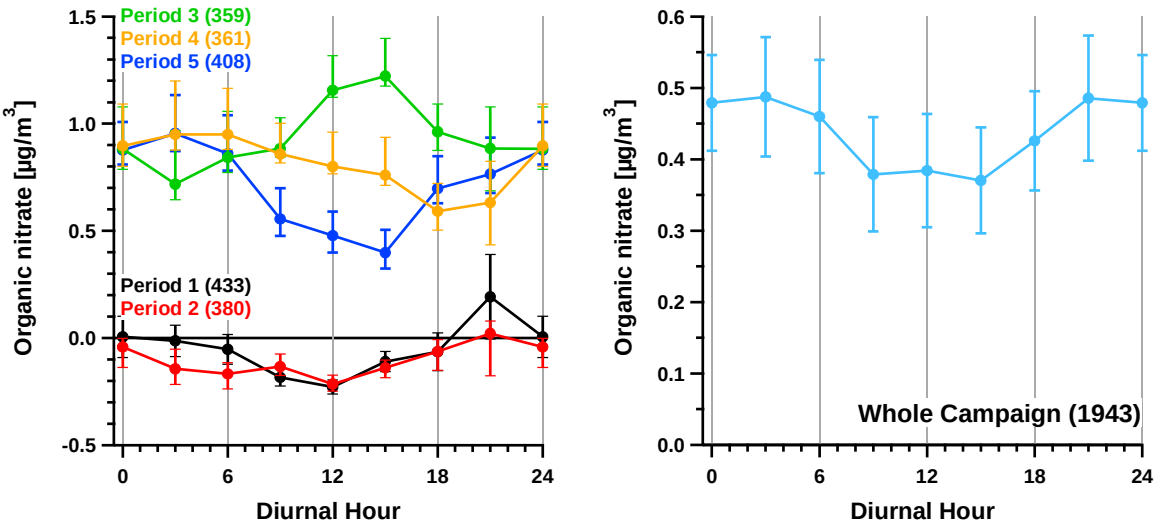

Figure S12: Average diurnal variations (LT) of the ACSM organic nitrate concentrations, calculated according to Sec. 3.2 in the main text. Concentrations are averaged over each period (left) and for the entire campaign (right), where the respective number of averaged data points is written in brackets. Error bars represent standard deviations of the mean values.

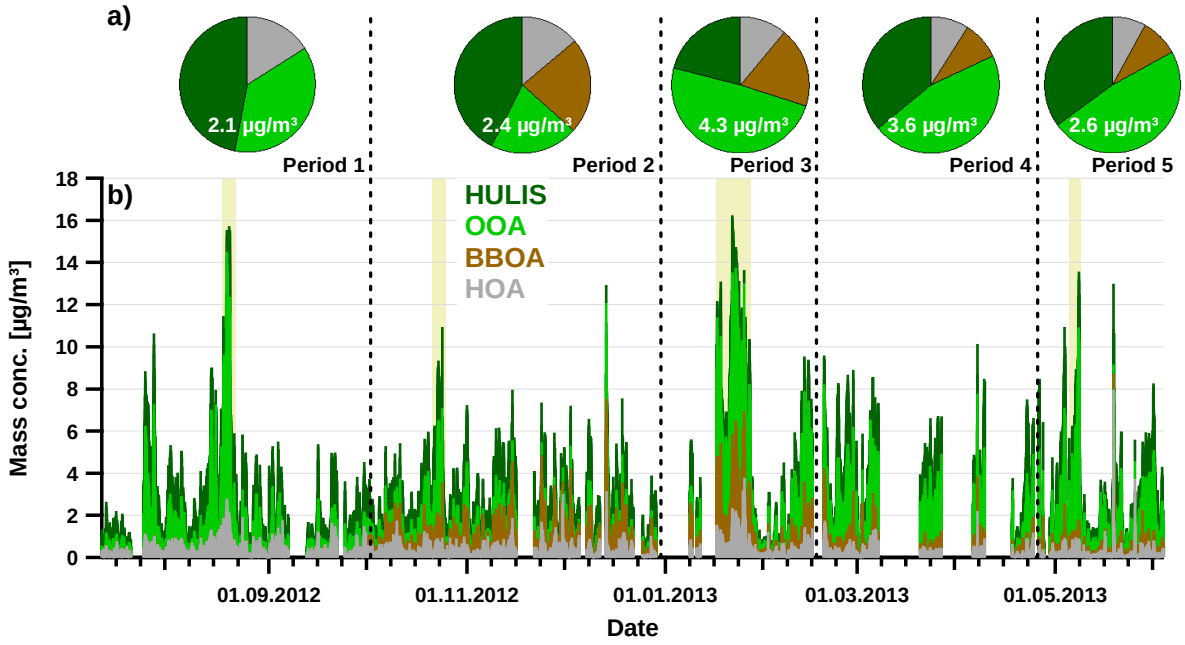

Figure S13: Overview of ACSM PMF factors: a) Pie charts of average fractional abundances of each factor, separated by the five periods as stated in Fig. 2 in the main text. The respective average total mass concentration is written inside the pie chart. b) Stacked time series of mass concentrations. Note that these plots were not obtained from one PMF exploration. Pollution events are indicated by shaded areas.

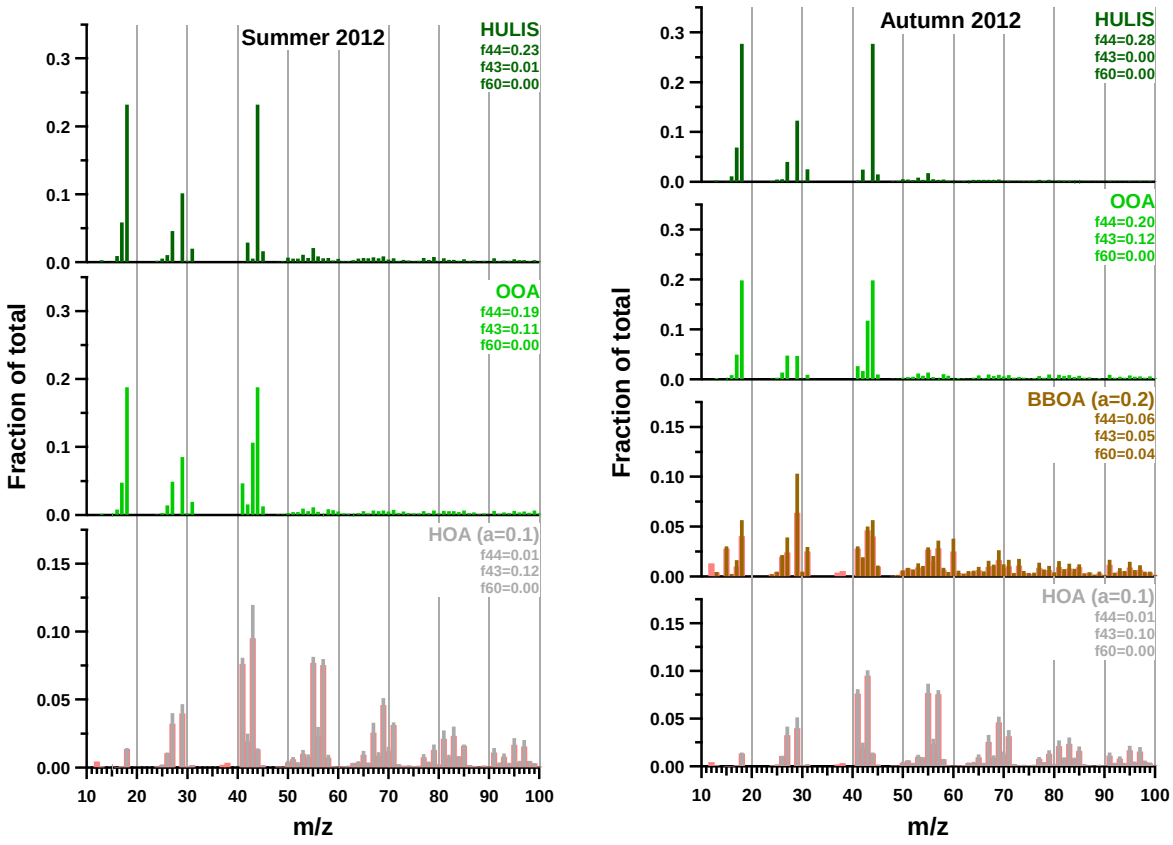

1

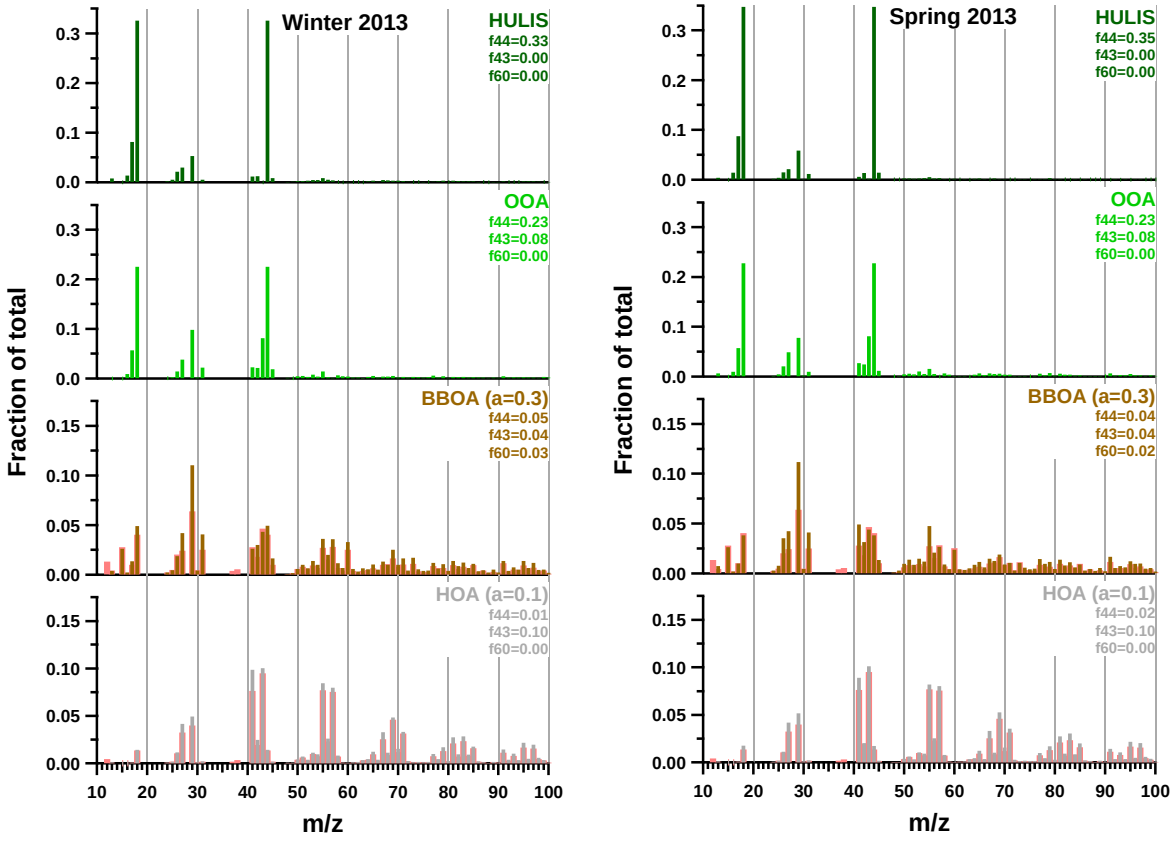

2

3 Figure S14: Mass spectra of ACSM PMF factors for each season between 2012 and 2013. For
4 the constrained profiles HOA and BBOA, the applied a-value is written in brackets.

Corresponding reference spectra are shown by red bars. *f44*, *f43*, and *f60* are the mass fractions of m/z 44, m/z 43, and m/z 60 of the particular MS, respectively. Note that the y-axis scales of the POA are zoomed by a factor of 2 comparing to SOA profiles.

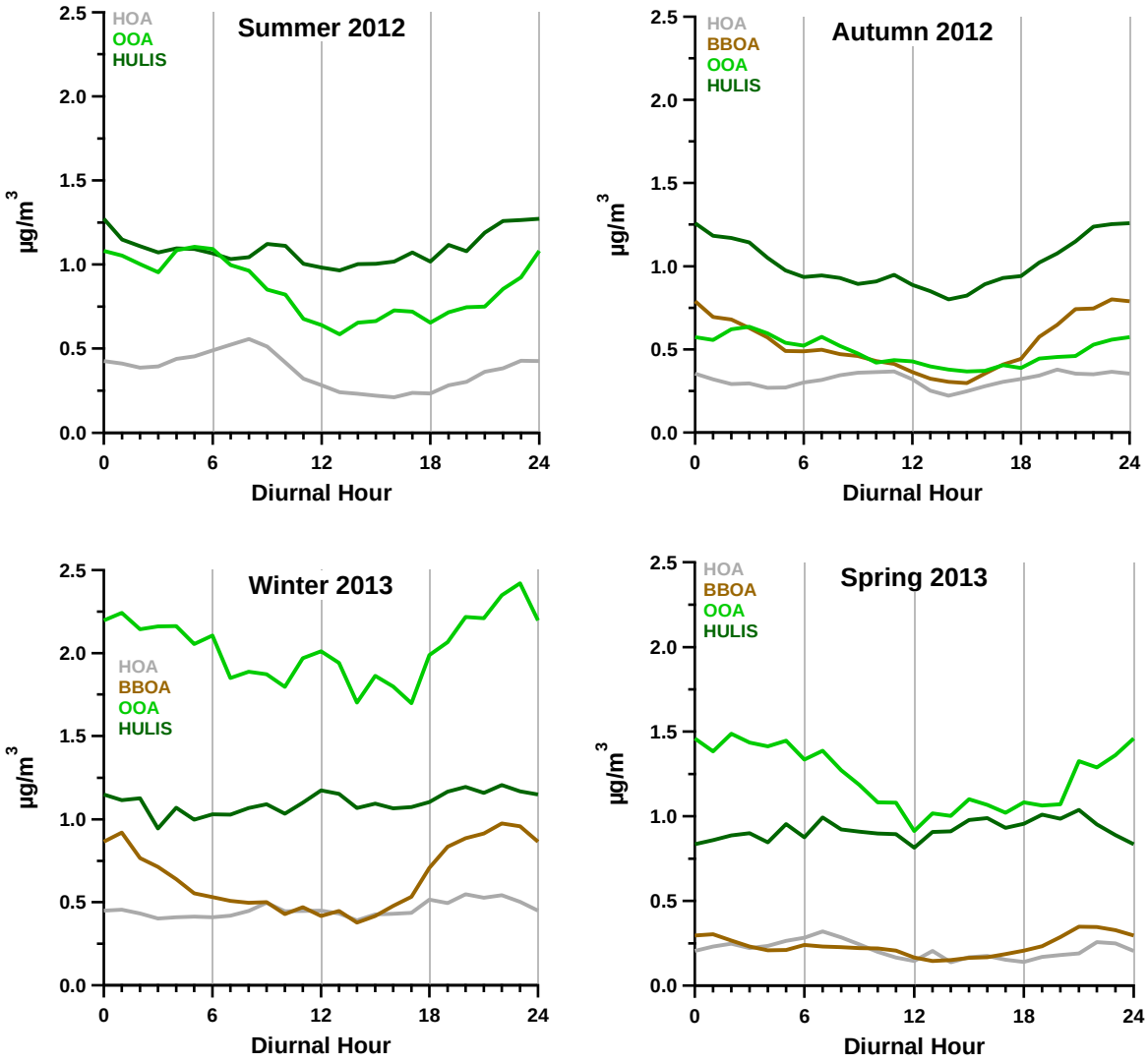

Figure S15: Average diurnal variations (local time) of ACSM PMF factors separated by season

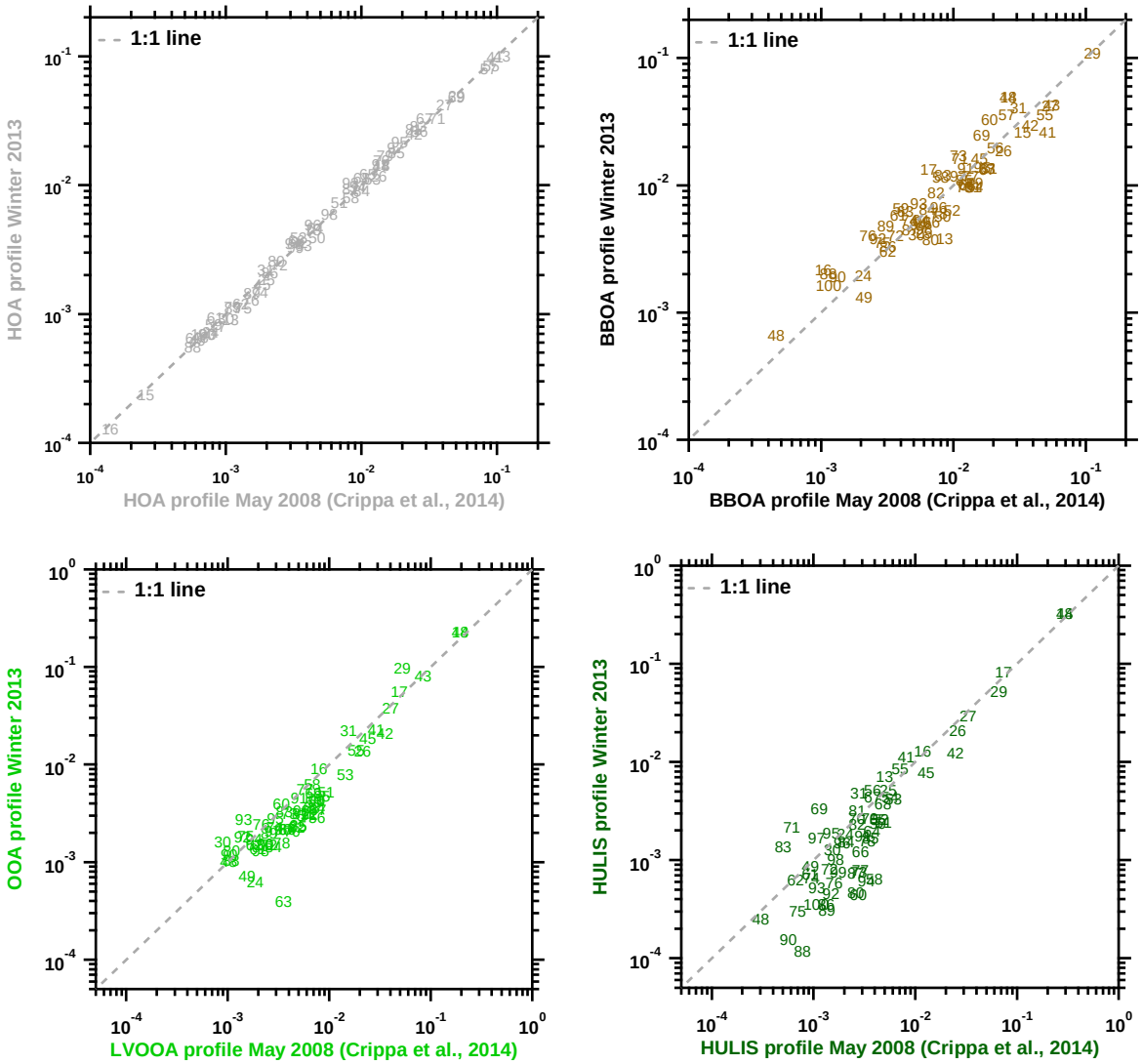

Figure S16: Scatter plots of PMF profiles from Winter 2013 vs. May 2008 as found by Crippa et al. (2014). Factor profiles from other seasons described in this work show similar correlations. The numerical markers correspond to m/z values.

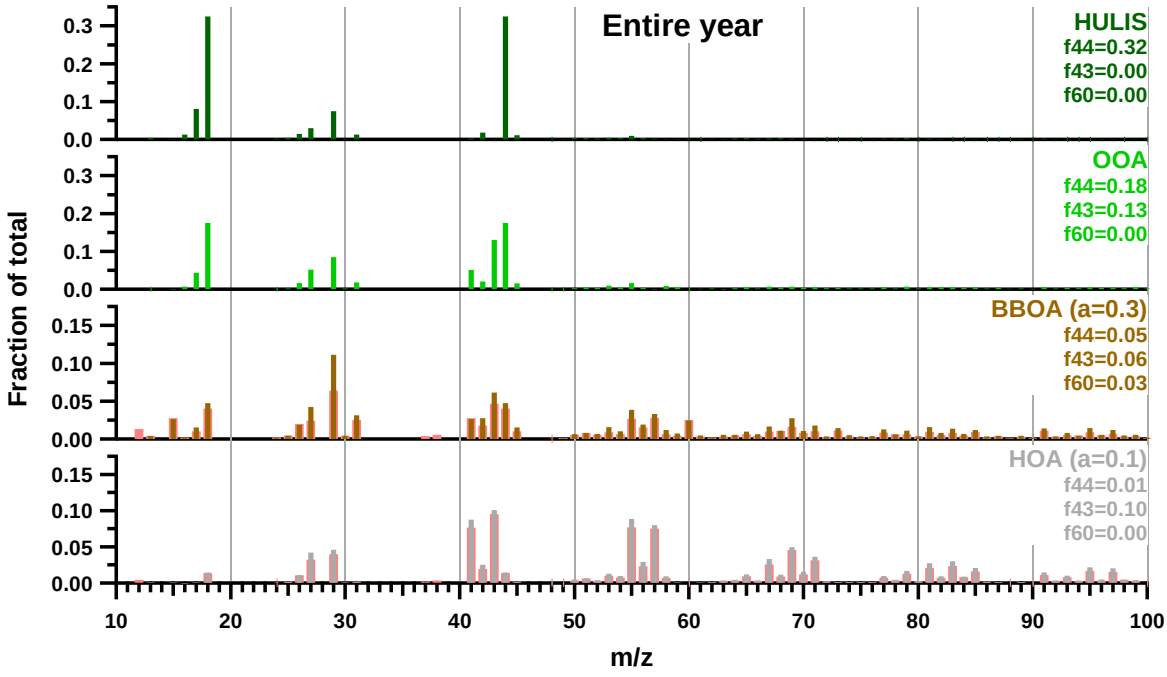

Figure S17: Mass spectra of ACSM PMF factors, derived from one single PMF exploration using the whole data set. For the constrained profiles HOA and BBOA, the applied a-value is written in brackets. Corresponding reference spectra are shown by red bars. *f44*, *f43*, and *f60* are the mass fractions of m/z 44, m/z 43, and m/z 60 of the particular MS, respectively. Note that the y-axis scales of the POA are zoomed by a factor of 2 comparing to SOA profiles.

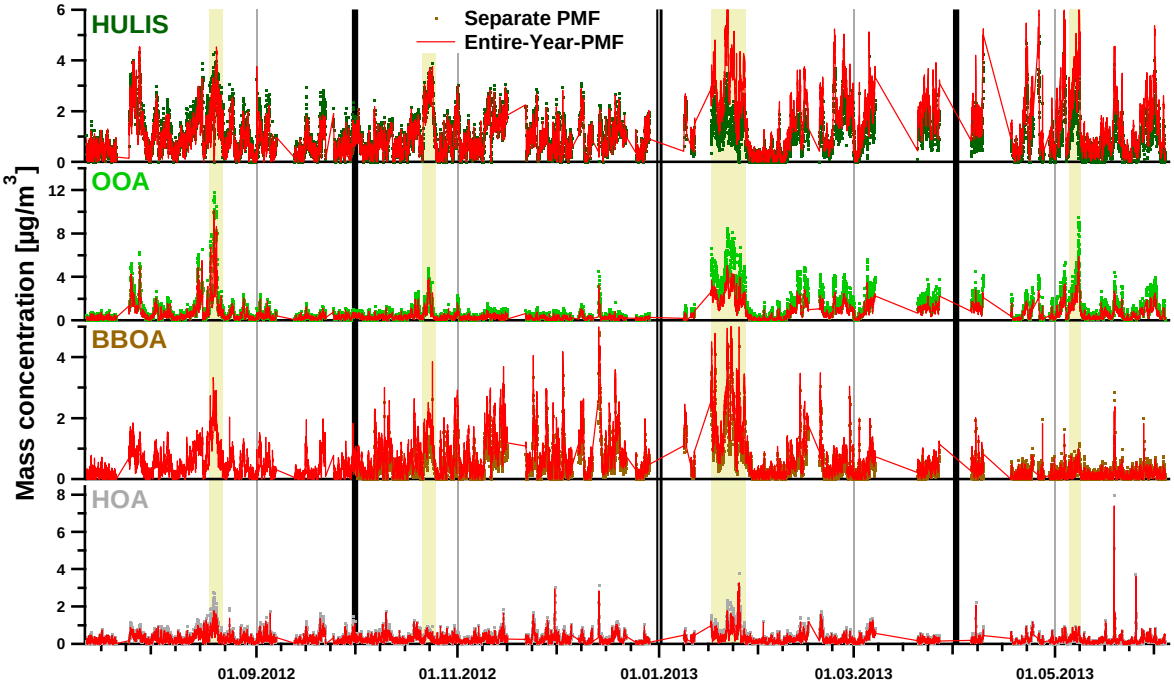

Figure S18: Time series of ACSM PMF factors. The dotted lines represent factors which are concatenated from separated solutions. Factors shown by red lines derived from one single PMF exploration using the whole data set. Pollution events are indicated by shaded areas. Vertical lines represent the division into the four seasons.

References

Crippa, M., Canonaco, F., Lanz, V.A., Äijälä, M., Allan, J.D., Carbone, S., Capes, G., Ceburnis, D., Dall'Osto, M., Day, D.A., DeCarlo, P.F., Ehn, M., Eriksson, A., Freney, E., Hildebrandt Ruiz, L., Hillamo, R., Jimenez, J.L., Junninen, H., Kiendler-Scharr, A., Kortelainen, A.-M., Kulmala, M., Laaksonen, A., Mensah, A.A., Mohr, C., Nemitz, E., O'Dowd, C., Ovadnevaite, J., Pandis, S.N., Petäjä, T., Poulain, L., Saarikoski, S., Sellegri, K., Swietlicki, E., Tiitta, P., Worsnop, D.R., Baltensperger, U., Prevot, A.S.H., 2014. Organic aerosol components derived from 25 AMS data sets across Europe using a consistent ME-2 based source apportionment approach. Atmospheric Chemistry and Physics 14, 6159-6176.

Mensah, A.A., Holzinger, R., Otjes, R., Trimborn, A., Mentel, T.F., ten Brink, H., Henzing, B., Kiendler-Scharr, A., 2012. Aerosol chemical composition at Cabauw, The Netherlands as observed in two intensive periods in May 2008 and March 2009. Atmospheric Chemistry and Physics 12, 4723-4742.

Vermeulen, A.T., Hensen, A., Popa, M.E., van den Bulk, W.C.M., Jongejan, P.A.C., 2011. Greenhouse gas observations from Cabauw Tall Tower (1992-2010). Atmospheric Measurement Techniques 4, 617-644.